AJNR

Dynamic Contrast-Enhanced MRI–Derived Intracellular Water Lifetime (τ_i): A Prognostic Marker for Patients with Head and Neck Squamous Cell Carcinomas

S. Chawla, L.A. Loevner, S.G. Kim, W.-T. Hwang, S. Wang, G. Verma, S. Mohan, V. LiVolsi, H. Quon and H. Poptani

Dynamic Contrast-Enhanced MRI–Derived Intracellular Water Lifetime (τ_i): A Prognostic Marker for Patients with Head and Neck Squamous Cell Carcinomas

S. Chawla, L.A. Loevner, S.G. Kim, W.-T. Hwang, S. Wang, G. Verma, S. Mohan, V. LiVolsi, H. Quon, and H. Poptani

ABSTRACT

BACKGROUND AND PURPOSE: Shutter-speed model analysis of dynamic contrast-enhanced MR imaging allows estimation of mean intracellular water molecule lifetime (a measure of cellular energy metabolism) and volume transfer constant (a measure of hemodynamics). The purpose of this study was to investigate the prognostic utility of pretreatment mean intracellular water molecule lifetime and volume transfer constant in predicting overall survival in patients with squamous cell carcinomas of the head and neck and to stratify p16-positive patients based upon survival outcome.

MATERIALS AND METHODS: A cohort of 60 patients underwent dynamic contrast-enhanced MR imaging before treatment. Median, mean intracellular water molecule lifetime and volume transfer constant values from metastatic nodes were computed from each patient. Kaplan-Meier analyses were performed to associate mean intracellular water molecule lifetime and volume transfer constant and their combination with overall survival for the first 2 years, 5 years, and beyond (median duration, >7 years).

RESULTS: By the last date of observation, 18 patients had died, and median follow-up for surviving patients ($n = 42$) was 8.32 years. Patients with high mean intracellular water molecule lifetime (4 deaths) had significantly ($P = .01$) prolonged overall survival by 5 years compared with those with low mean intracellular water molecule lifetime (13 deaths). Similarly, patients with high mean intracellular water molecule lifetime (4 deaths) had significantly ($P = .006$) longer overall survival at long-term duration than those with low mean intracellular water molecule lifetime (14 deaths). However, volume transfer constant was a significant predictor for only the 5-year follow-up period. There was some evidence ($P < .10$) to suggest that mean intracellular water molecule lifetime and volume transfer constant were associated with overall survival for the first 2 years. Patients with high mean intracellular water molecule lifetime and high volume transfer constant were associated with significantly ($P < .01$) longer overall survival compared with other groups for all follow-up periods. In addition, p16-positive patients with high mean intracellular water molecule lifetime and high volume transfer constant demonstrated a trend toward the longest overall survival.

CONCLUSIONS: A combined analysis of mean intracellular water molecule lifetime and volume transfer constant provided the best model to predict overall survival in patients with squamous cell carcinomas of the head and neck.

ABBREVIATIONS: CRT = chemoradiation therapy; DCE-MRI = dynamic contrast-enhanced MR imaging; HNSCC = squamous cell carcinomas of the head and neck; HPV = human papillomavirus; HR = hazard ratio; K^{trans} = volume transfer constant; OS = overall survival; τ_i = mean intracellular water molecule lifetime

Patients with squamous cell carcinomas of the head and neck (HNSCC) are usually associated with a poor prognosis, and the presence of metastatic lymph nodes is considered a negative prognostic indicator.[1] Consequently, there is an unmet need to understand the tumor biology to improve clinical management.

Dynamic contrast-enhanced MR imaging (DCE-MRI) allows estimation of volume transfer constant (K^{trans}),[2,3] an efflux rate constant of gadolinium-based contrast agent from the intravas-

cular compartment to tumor interstitium. The potential of pretreatment K^{trans} in predicting short-term response[4-7] as well as overall survival (OS) in patients with HNSCC has been reported.[8,9] Patients treated with chemoradiation therapy (CRT) and with high baseline K^{trans} from metastatic nodes were associated with an improved prognosis compared with patients with low baseline K^{trans}.[8,9] In addition to K^{trans}, shutter-speed model analysis of DCE-MRI derives a novel imaging biomarker known as mean intracellular water lifetime (τ_i),[10-12] which has been suggested to be a metabolic marker.[12] The unique strength of τ_i lies in the fact that it is less sensitive to arterial input function scaling variations than K^{trans},[13] indicating that τ_i is a more reproducible and reliable marker. The parameter τ_i has been used to characterize breast,[14] prostate,[15,16] esophageal,[17] and hepatocellular cancer.[18] A recent study[19] also demonstrated the prognostic utility of τ_i in predicting survival in patients with hepatocellular carcinomas.

Although K^{trans} reflects tumor perfusion and vascular permeability,[3] τ_i provides unique information related to tumor cell characteristics such as cell size, cell membrane permeability, and cellular metabolic activity.[12] Given that K^{trans} and τ_i provide complementary information about the tumor microenvironment, we believe that a combined analysis may be more useful than individual parameters in predicting prognosis in patients with HNSCC.

Thus, the purpose of the present study was to assess the prognostic value of pretreatment τ_i and K^{trans} in predicting OS in patients with HNSCC. In addition, in a subset of patients, we explored the prognostic potential of τ_i and K^{trans} in p16-associated HNSCC given the fundamental differences in tumor biology and prognosis of these patients.[20-22]

MATERIALS AND METHODS
Patients
This retrospective analysis of pre-existing imaging and clinical data was institutional review board–approved and was compliant with the Health Insurance Portability and Accountability Act. On the basis of previous CT/MR imaging reports, all patients were assessed for the presence of at least 1 metastatic cervical lymph node measuring >1 cm³ and biopsy-proved histopathologic diagnosis of HNSCC. The exclusion criteria included prior CRT or a history of cancer other than HNSCC. A total of 72 patients with newly diagnosed HNSCC met the inclusion criteria and were recruited between January 2005 and August 2009. TNM staging was used to determine the disease status. Each patient received appropriate therapy to deliver the maximum clinical benefit, which included upfront neck dissection ($n = 3$), concurrent CRT ($n = 46$), or induction chemotherapy followed by CRT ($n = 23$). Three patients who underwent upfront neck dissection and 9 patients who had either corrupted MR imaging data or insufficient clinical data were excluded from the data analysis. Therefore, OS analyses were performed on the remaining 60 patients (mean age ± SD, 62.34 ± 9.18 years; 49 men, 11 women). Tumor location and staging from these patients at the initial presentation are summarized in the Table.

Data Acquisition
All patients underwent MR imaging before surgery and CRT on a 1.5T Sonata scanner (Siemens, Erlangen, Germany; $n = 37$) or on

Patient characteristics and treatment modalities

Characteristics	
Number of patients	60
Mean age, yrs ± SD	62.34 ± 9.18
Sex	
Male	49 (81.7%)
Female	11 (18.3%)
Primary tumor site	
Base of tongue	24 (40.0%)
Tonsil	14 (23.3%)
Larynx	7 (11.7%)
Less common/unknown sites	15 (25.0%)
T staging	
Tx	14 (23.3%)
T0	2 (3.3%)
T1	2 (3.3%)
T2	15 (25.0%)
T3	9 (15.0%)
T4	18 (30.0%)
N staging	
N1	2 (3.3%)
N2	51 (85.0%)
N3	7 (11.7%)
M staging	
M0	60 (100%)
p16 expression	
Positive	21 (35.0%)
Negative	11 (18.3%)
Unknown (insufficient specimen)	28 (46.7%)
Treatment	
Radiotherapy + concurrent chemotherapy	39 (65.0%)
Induction chemotherapy + radiotherapy + concurrent chemotherapy	21 (35.0%)

a 3T Magnetom Trio scanner (Siemens; $n = 35$). Structural imaging included axial T2-weighted and T1-weighted images with standard parameters. Inversion-recovery–prepared T1-weighted images were acquired by using TIs of 60, 200, 400, 800, and 1600 ms before the acquisition of DCE-MRI data for T1 quantification.

As described previously,[5] DCE-MRI was performed by using a rapid 3D-spoiled gradient-echo sequence modified to acquire 8 angle-interleaved subaperture images from the full-echo radial data.[23] Imaging parameters were: TR, 5.0 ms; TE, 4.2 ms; 256 readout points per view; 256 views (32 views per subaperture, 8 subapertures); field of view, 260 × 260 mm²; number of sections, 8; section thickness, 5 mm. Fat saturation was applied once every 8 excitations. Spatial saturation was applied once every 32 excitations to minimize the flow effect while minimizing acquisition time. This scheme resulted in a temporal resolution of 2.5 seconds for each subaperture image with full spatial resolution of 256 × 256 by using a dynamic k-space–weighted image reconstruction contrast algorithm.

Image Processing
All images (T2, T1, postcontrast T1-weighted, and DCE-MRI) were coregistered by using a 2-step nonrigid image registration technique.[5] The ROIs were drawn on the solid portion of the largest nodal mass by using anatomic images. Care was taken to avoid necrotic/cystic or hemorrhagic parts as well as surrounding blood vessels. Pharmacokinetic analysis of DCE-MRI data was performed for each voxel in the selected ROIs by using a shutter-speed model.[5,10] Estimation of arterial input function was per-

formed semiautomatically from an ROI on one of the carotid arteries located near the metastatic lymph node.[5,10] Median pretreatment τ_i and K^{trans} were computed by using only the central 4 sections to avoid erroneous results from wraparound artifacts in the edge sections.

Clinical Follow-Up and Data Analysis

The clinical follow-up period was measured from the end date of CRT to the date of death for deceased patients or to the date of last observation for surviving patients.

Median pretreatment τ_i and K^{trans} values were 0.125 seconds and 0.409 minutes^{-1}, respectively, and were used as thresholds to divide patients into 2 groups (at or above and below the threshold value). Patients in the high τ_i group had a mean $\pm$ SD τ_i of 0.276 $\pm$ 0.086 seconds and a median of 0.269 seconds. Patients in the low τ_i group had a mean $\pm$ SD τ_i of 0.070 $\pm$ 0.028 seconds and a median of 0.071 seconds. Similarly, patients in the high K^{trans} group had a mean $\pm$ SD K^{trans} of 0.90 $\pm$ 0.54 minutes^{-1} with a median of 0.88 minutes^{-1}, whereas patients in the low K^{trans} group had a mean $\pm$ SD K^{trans} of 0.188 $\pm$ 0.108 minutes^{-1} and a median of 0.196 minutes^{-1}.
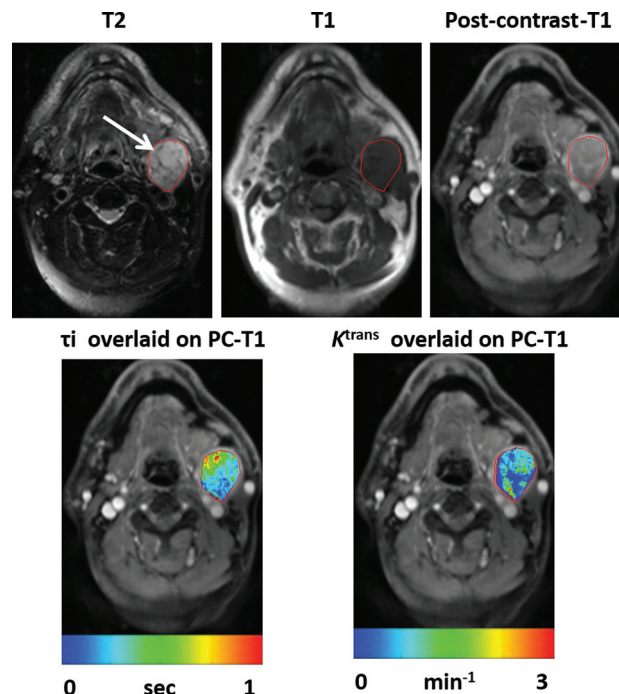
Using the 2-year (short-term), 5-year (intermediate-term), and all available follow-up (long-term [median, 7.83 years; range, 0.07–10.7 years]) as clinical end points, OS was analyzed. In addition to using τ_i and K^{trans} as independent predictors, combinations of these parameters (high τ_i/high K^{trans}, high τ_i/low K^{trans}, low τ_i/high K^{trans}, and low τ_i/low K^{trans}) were used. Kaplan-Meier survival curves were plotted and compared by using log-rank tests. Using a Cox regression model, hazard ratios (HRs) of deaths and associated 95% CI were estimated for τ_i and K^{trans} first separately, and then for the different combinations of these parameters (high τ_i/high K^{trans}, high τ_i/low K^{trans}, low τ_i/high K^{trans}, and low τ_i/low K^{trans}). In addition, a Wald test was performed to evaluate the joint effect of these combinations. A P value <.05 was considered significant. All data analyses were performed by using SPSS for Windows version 18.0 (IBM, Armonk, New York).

Stratifying HPV/p16-Positive and p16-Negative Patients

Human papillomavirus (HPV) status was determined from tissue specimens by immunohistochemical evaluation of p16 expression by using a commercially available monoclonal antibody. Tissue samples were available from only 32 patients, and these were divided into 2 groups: positive ($n = 21$) or negative ($n = 11$) for p16 expression.[24] There were no significant differences ($P > .05$) in age, treatment regimen, τ_i, and K^{trans} between patients who had and those who did not have tissue specimens for p16 expression. Using p16 as an independent variable, OS analyses were performed from these 32 patients. To further stratify p16-positive and p16-negative patients, separate OS analyses were performed by using τ_i and K^{trans} as independent variables and by using combinations of these parameters.

RESULTS

Representative anatomic images and τ_i and K^{trans} maps from a patient who was alive by the last date of observation with a follow-up duration of 8.19 years and from a patient who died 2.12 years after the end of CRT are shown in Figs 1 and 2, respectively.

| T2 | T1 | Post-contrast-T1 |

τi overlaid on PC-T1 K^{trans} overlaid on PC-T1

0 sec 1   0 min^{-1} 3

FIG 1. Representative images from a patient exhibiting long survival (follow-up duration of 8.19 years). Axial T2-weighted image (*A*) demonstrates an enlarged heterogeneous hyperintense metastatic left level IIa lymph node (*arrow*). This appears hypointense on a coregistered T1-weighted image (*B*), with heterogeneous enhancement on the corresponding postcontrast T1-weighted image (*C*). DCE-MRI–derived τ_i (0.136 seconds [*D*]) and K^{trans} (0.882 minutes^{-1} [*E*]) maps are shown as color images overlaid on postcontrast T1-weighted images.

In the first 2-year follow-up period, 13 of 60 patients died of the disease. In 5 years, the number of deceased patients was 17, whereas a total of 18 patients died by the last date of observation. The median follow-up for surviving patients ($n = 42$) was 8.32 years (range, 5.42–10.7 years).

Prognostic Utility of τ_i

In the first 2 years, a trend toward longer OS was noted for patients with higher τ_i (4 deaths) compared with those with lower τ_i (9 deaths; log-rank $P = .09$). The probability for survival in patients with high τ_i was 86.7% (95% CI, 68.3%–94.8%), whereas it was 70% (95% CI, 60.3%–83.1%) for patients with low τ_i.

Interestingly, by 5 years, significantly longer OS was observed for patients with higher τ_i (4 deaths) compared with those with lower τ_i (13 deaths; log-rank $P = .01$). Similarly, patients with higher τ_i (4 deaths) had significantly prolonged OS compared with those with lower τ_i (14 deaths; log-rank $P = .006$; Fig 3) when long-term follow-up duration was considered (median duration, >7 years). At 5 years, survival probability for patients with high τ_i was 86.7% (95% CI, 68.3%–94.8%), and for patients with low τ_i, it was 56.8% (95% CI, 37.4%–72.1%).

Cox regression analysis demonstrated a nonsignificant difference ($P = .13$) in OS between the 2 groups for the 2-year follow-up period, with an HR of 2.43 (95% CI, 0.75–7.92). However, a P value of .02 with HR of 3.71 (95% CI, 1.20–11.39) for 5 years and a P value of .01 with HR of 4.24 (95% CI, 1.38–12.97) were observed in predicting long-term OS.
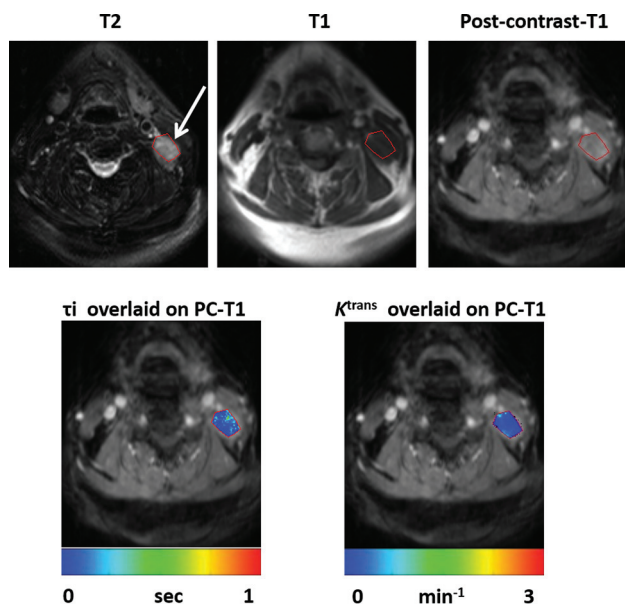
FIG 2. Representative images from a patient who died 2.12 years after the end of CRT. Axial T2-weighted image (*A*) demonstrates a heterogeneous hyperintense metastatic left level IIb lymph node (*arrow*). It appears hypointense on a coregistered T1-weighted image (*B*) with heterogeneous enhancement on postcontrast T1-weighted image (*C*). DCE-MRI– derived τ_i (0.031 seconds; [*D*]) and K^{trans} (0.135 minutes^{-1} [*E*]) maps overlaid on postcontrast T1-weighted images demonstrating lower τ_i and K^{trans} values from the node compared with the patient with longer survival as shown in Fig 1.
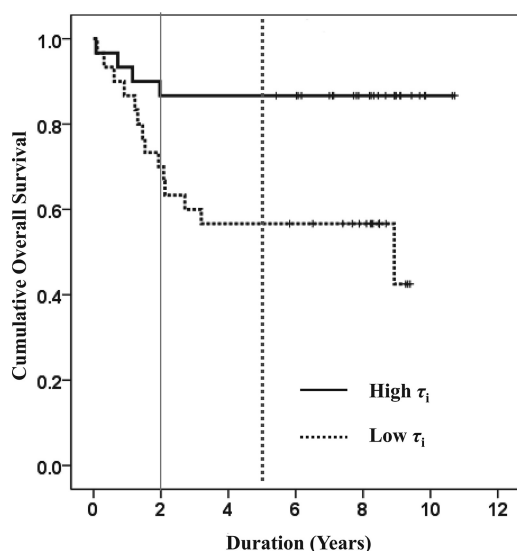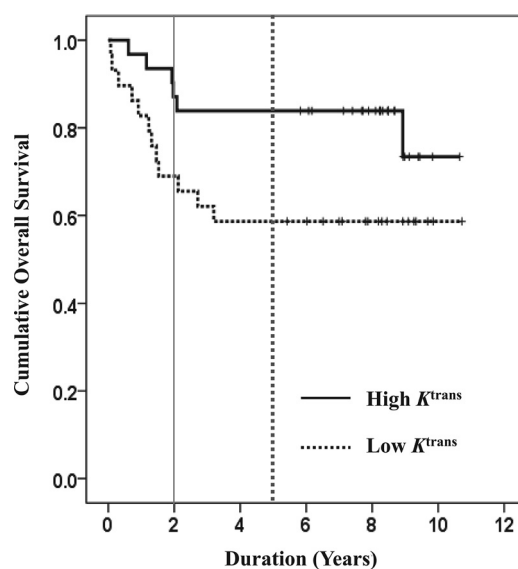

FIG 3. Kaplan-Meier plot for τ_i. Patients with higher pretreatment τ_i (*solid curves*) demonstrate longer OS compared with patients with lower τ_i (*broken curves*) for first 2-year (solid vertical line, $P = .09$), 5-year (dotted vertical line, $P = .01$), and long-term (median duration, >7 years; $P = .006$) follow-up periods.

Prognostic Utility of K^{trans}

At 2 years, patients with higher K^{trans} (4 deaths) had longer but nonsignificant OS compared with those with lower K^{trans} (9 deaths; log-rank $P = .07$). At 2 years, survival probability was 87.1% (95% CI, 69.2%–95.0%) for patients with high K^{trans} and 69.0% (95% CI, 48.8%–82.5%) for patients with low K^{trans}.

By 5 years, significantly prolonged OS for patients with higher K^{trans} (5 deaths) was noted compared with those with lower K^{trans}

FIG 4. Kaplan-Meier plots for K^{trans}. Patients with higher pretreatment K^{trans} (*solid curves*) demonstrate longer OS compared with patients with lower K^{trans} (*broken curves*) at the 2-year (*solid vertical line*; $P = .07$), 5-year (*dotted vertical line*; $P = .028$), and long-term (median duration, >7 years; $P = .06$) follow-up periods.

(12 deaths; log-rank $P = .03$). Survival probability for patients with high K^{trans} was 83.9% (95% CI, 65.5%–93.0%) and for patients with low K^{trans} was 58.6% (95% CI, 38.8%–74.0%). However, only a trend toward prolonged OS was observed for patients with higher K^{trans} (6 deaths) compared with those with lower K^{trans} (12 deaths; log-rank $P = .06$) when long-term OS was evaluated (Fig 4).

Cox regression analyses showed nonsignificant differences between the 2 groups for 2 years ($P = .09$) with HR of 2.78 (95% CI, 0.85–9.05) and for long-term periods ($P = .06$) with HR of 2.52 (95% CI, 0.94–6.72). However, a P value of .04 with HR of 3.04 (95% CI, 1.07–8.64) was observed in predicting 5-year OS.

Prognostic Utility of Combined Analysis Involving τ_i and K^{trans}

By 2 years, the longest OS was observed for patients with high τ_i/high K^{trans} ($n = 15$, 2 deaths). On the other hand, patients with low τ_i/low K^{trans} ($n = 14$, 7 deaths) had the shortest OS (log-rank $P = .02$). In the group of patients ($n = 31$) who had either high τ_i/low K^{trans} or low τ_i/high K^{trans}, 4 patients died. Moreover, patients with high τ_i/low K^{trans} had longer OS than patients with low τ_i/high K^{trans}. Similarly, at 5 years, patients with high τ_i/high K^{trans} ($n = 15$, 2 deaths) had the longest OS, whereas patients with low τ_i/low K^{trans} ($n = 14$, 10 deaths) had the shortest OS (log-rank $P < .0001$). Of the remaining 31 patients, 5 patients were deceased and patients with high τ_i/low K^{trans} had longer OS than patients with low τ_i/high K^{trans}.

A similar pattern was observed for long-term analysis. Patients with high τ_i/high K^{trans} ($n = 15$, 2 deaths) had the longest OS, and patients with low τ_i/low K^{trans} ($n = 14$, 10 deaths) had the shortest OS (log-rank $P < .0001$). Of the remaining 31 patients, 6 died, and again, patients with high τ_i/low K^{trans} had longer OS than patients with low τ_i/high K^{trans} (Fig 5).

For the first 2-year follow-up period, multivariate Cox regression analyses revealed a P value of .048 with HRs of 0.21 (95% CI, 0.04–1.00; $P = .05$), 0.22 (95% CI, 0.05–1.07; $P = .06$), and 0.20 (95% CI, 0.04–0.95; $P = .04$) for patients with high τ_i/high K^{trans}, high τ_i/low K^{trans}, and low τ_i/high K^{trans}, respectively, with respect to patients with low τ_i/low K^{trans}. Similarly, a P value of .003 with HRs of 0.13 (95% CI, 0.03–0.60; $P = .009$), 0.14 (95% CI, 0.03–0.63; $P = .01$), and 0.19 (95% CI, 0.05–0.69; $P = .01$) for the first 5 years, and P value of .003 with HRs of 0.12 (95% CI, 0.03–0.58;

$P = .007$), 0.13 (95% CI, 0.03–0.61; $P = .01$), and 0.26 (95% CI, 0.08–0.82; $P = .02$) for long-term OS were observed.

When all the combinations of variables (high τ_i/high K^{trans}, high τ_i/low K^{trans}, low τ_i/high K^{trans}) were considered together, HRs of 1.84 (95% CI, 1.05–3.23; $P = .03$), 2.32 (95% CI, 1.35–3.97; $P = .002$), and 2.31 (95% CI, 1.38–3.87; $P = .001$) for the first 2 years, 5 years, and long-term OS, respectively, were observed. Overall, combination of the τ_i and K^{trans} groups demonstrated differential OS (Wald test, $P = .003$).

Stratifying HPV/p16-Positive and p16-Negative Patients

Of 32 patients with the availability of p16 status, 13 died by the date of last observation. Patients with p16-positive status had significantly longer OS than p16-negative patients ($P = .05$; Fig 6A). Noticeably, no significant difference ($P = .17$) in OS was observed between patients in whom p16-expression data were or were not available.
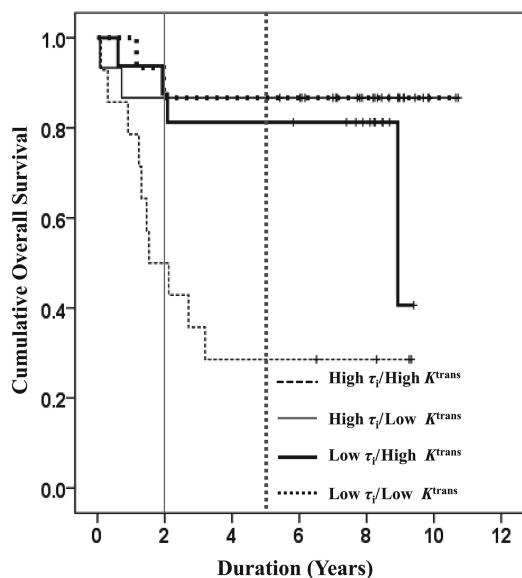
Patients with p16-positive status with higher τ_i demonstrated nonsignificantly longer OS ($P = .20$) than patients with lower τ_i. Similarly, nonsignificant ($P = .61$) differences were observed for K^{trans}. Moreover, p16-positive patients with high τ_i/high K^{trans} had the longest OS, and patients with low τ_i/low K^{trans} had the shortest OS. However, these findings were also not significant (Fig 6B; $P > .05$). In addition, patients with p16-negative status and higher τ_i demonstrated nonsignificantly ($P = .12$) longer OS than those with lower τ_i. We could not compare OS by using K^{trans} because all patients in this subgroup had K^{trans} higher than the median value.

FIG 5. Kaplan-Meier plots for combinations of τ_i and K^{trans}. Patients with high τ_i/K^{trans} (*thick broken curve*) had the longest OS, and patients with low τ_i/K^{trans} (*thin broken curve*) had the shortest OS for the first 2-year (*solid vertical line*; $P = .02$), 5-year (*dotted vertical line*; $P < .0001$), and long-term (median duration, >7 years; $P < .0001$) follow-up periods. In addition, patients with high τ_i/low K^{trans} (*thick solid curve*) exhibited longer OS than patients with low τ_i/high K^{trans} (*thin solid curve*) at all clinical end points.
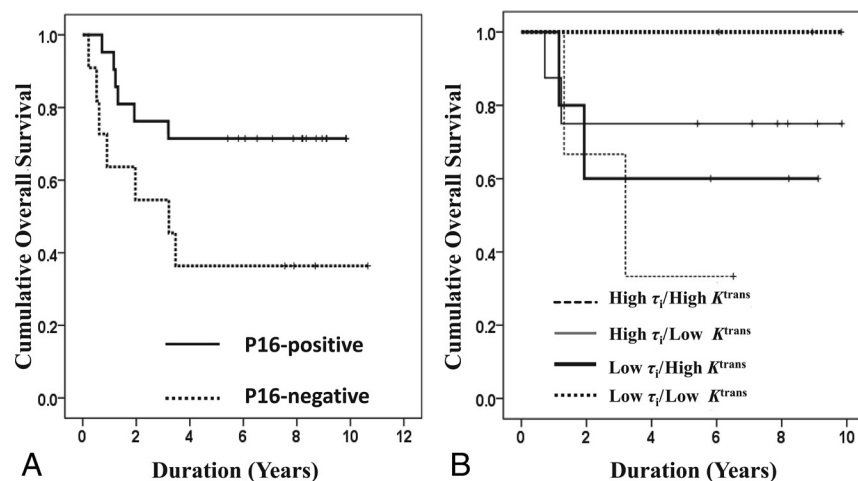
FIG 6. Kaplan-Meier plots for p16 expression. (*A*) Patients with p16-positive expression (*solid curve*) exhibited significantly longer long-term (median duration, >7 years) OS ($P < .05$) than patients with p16-negative expression (*broken curve*) (*B*). Patients with positive p16 expression and high τ_i/high K^{trans} (*thick broken curve*) had longer OS than p16-positive patients with low τ_i/low K^{trans} (*thin broken curve*). In addition, patients with high τ_i/low K^{trans} (*gray solid curve*) exhibited longer OS than patients with low τ_i/high K^{trans} (*black solid curve*) at all clinical end points. However, these differences were not significant ($P > .05$).

DISCUSSION

Our observations suggest that patients with higher pretreatment τ_i and K^{trans} from metastatic nodes exhibit longer OS. These results are particularly encouraging given the adverse prognosis associated with nodal metastases and offer potential opportunities to develop alternative therapeutic approaches in the poor prognosis cohort.

Earlier studies[12,25,26] have reported that τ_i is inversely correlated with cell membrane ion-pump activity, a measure of mitochondrial metabolism suggesting that τ_i might be a sensitive indicator of cellular energy turnover. Similarly, some studies have reported that increased metabolic activity is associated with lower τ_i (median, 0.16–1.03 seconds) in regions of prostate[15,16] and esophageal cancer[17] compared with normal tissues. In yet another study,[18] lower τ_i (0.11 ± 0.02 seconds versus 0.29 ± 0.53 seconds) was observed from normal liver parenchyma (a metabolically more active region) compared with hepatocellular carcinomas. The inverse correlation between τ_i and tumor metabolism was corroborated when higher τ_i was observed in complete responders compared with poor responders with breast carcinomas.[12,14] Taken together, these studies imply that malignant cells

from tumors with high τ_i have reduced metabolic energy available for their growth relative to malignant cells from tumors with low τ_i.

In the present study, patients with HNSCC with higher pretreatment τ_i from the metastatic nodes were associated with prolonged OS measured at 3 different clinical end points, suggesting that malignant cells were associated with reduced metabolic energy. An inverse correlation of τ_i with EF5, a marker of hypoxia, and direct correlation of elevated τ_i regions with high blood flow have been reported.[27] An earlier study[28] reported that tumors with relatively higher blood flow and reduced hypoxia are associated with increased oxygenation, resulting in better access to chemotherapeutic drugs and radiosensitity. Taken together, these studies and our observations suggest that tumors with higher τ_i may harbor a favorable microenvironment for CRT. We postulate that the combined effect of lower hypoxia and reduced metabolic activity of the tumor cells might have contributed to higher pretreatment τ_i that led to better treatment response and prolonged OS in patients with HNSCC. This notion is supported by a HR of 4.24 that was observed at the long-term follow-up period, implying a 4-fold higher risk of death in patients with low τ_i than in patients with high τ_i.

Pretreatment K^{trans} (median value, $0.19 - 0.64$ minutes^{-1}) has been reported to predict treatment response to CRT,[4-6] induction therapy,[7] and short-term survival in patients with HNSCC.[8,9] We also observed that higher pretreatment K^{trans} was associated with better OS. Because K^{trans} reflects a combination of tumor perfusion and microvascular permeability, our results and those of earlier published reports support the notion that tumor vascularity might be an important predictor of disease control in HNSCC. The fact that K^{trans} predicted only 5-year OS while τ_i was useful in predicting both 5-year and long-term OS suggests that τ_i is a more robust prognostic imaging biomarker in evaluating HNSCC.

When τ_i and K^{trans} were combined, significantly longer OS was observed for patients with high τ_i/high K^{trans} for all clinical end points. We believe that synergistic interaction between these 2 parameters in predicting OS was greater than what would be expected from an individual parameter. The fact that patients with high τ_i/high K^{trans} demonstrated the longest OS agrees with the hypothesis that these patients may have had the most favorable conditions such as elevated tumor blood flow, lower hypoxia, and lower cellular metabolic energy for optimal therapeutic benefit of CRT. Another interesting finding was that patients with high τ_i/low K^{trans} exhibited longer OS than patients with low τ_i/high K^{trans} at all clinical end points. This indicates that τ_i was a more dominant factor than K^{trans} in the synergistic interaction leading to longer OS, further substantiating that τ_i is a robust prognostic indicator in HNSCC.

We performed an exploratory analysis to investigate if τ_i and K^{trans} could predict OS in HPV/p16 patients because HPV/p16 is a key etiological factor in HNSCC, with distinct epidemiologic, clinical, and molecular characteristics.[21,22] Patients harboring the p16 gene are generally more sensitive to CRT and are associated with improved prognosis and prolonged survival.[20] The favorable outcome in p16-positive patients may be attributed to fewer and distinct somatic genetic alterations and positive immunologic response.[21,22] In agreement with prior studies,[20,21] significantly

longer OS was observed for p16-positive patients compared with p16-negative patients in our study. A nonsignificant, but positive trend toward longer OS for p16-positive patients harboring high τ_i and K^{trans} suggests the prognostic utility of τ_i and K^{trans} may also be valid in stratifying p16-positive patients. We recognize that these results may be subject to selection bias inherent to the availability of tissue specimens. However, a nonsignificant difference in OS between patients who had and those who did not have tissues for p16 expression indicated that there was a minimal influence of sample size in the determination of OS.

While predicting short-term (6 months) treatment response to CRT, no significant differences in pretreatment τ_i were observed between complete and partial responders.[5] However, in the present study, patients who had higher pretreatment τ_i were associated with prolonged OS. The difference might be related to different follow-up duration, assessment of clinical outcome (local regional recurrence/evidence of residual disease on pathology versus OS), and different number of patients ($n = 33$ versus $n = 60$) enrolled between these 2 studies. We focused on assessing nodal metastases in predicting OS because lymphadenopathy in the neck is a well-known prognostic determinant in patients with HNSCC.[29] A DCE-MRI analysis of primary tumors would also be important; however, artifacts induced by physiologic motion precluded the analysis of primary tumors. We combined DCE-MRI data from MR systems with 2 different field strengths (1.5T and 3T). To account for this variability, blood T1 and contrast agent relaxivities corresponding to the field strengths were used for converting signal intensity curves to concentration curves and estimating pharmacokinetic parameters. Previously,[5] we reported similar trends for K^{trans} in predicting treatment response in patients scanned at 2 different field strengths, suggesting that DCE-MRI–derived parameters are independent of magnetic field. Our supposition is corroborated by a study[30] in which no significant differences in signal enhancement ratio, time to peak enhancement, uptake, and washout rates were observed for breast lesions scanned with 1.5T and 3T MR systems.

CONCLUSIONS

Our data indicate that shutter-speed model analysis of DCE-MRI provides 2 important imaging biomarkers (τ_i and K^{trans}) presenting complementary physiologic information about the tumor microenvironment. Although τ_i may be a potential independent prognostic imaging biomarker for predicting OS, combined analysis of τ_i and K^{trans} greatly improves the predictive power of these parameters in determining OS in HNSCC. Future prospective trials involving a larger patient population are required to confirm our findings.

REFERENCES

1. Chen CC, Lin JC, Chen KW. **Lymph node ratio as a prognostic factor in head and neck cancer patients.** *Radiat Oncol* 2015;10:181 CrossRef Medline

2. Tofts PS, Kermode AG. **Measurement of the blood-brain barrier permeability and leakage space using dynamic MR imaging. 1. Fundamental concepts.** *Magn Reson Med* 1991;17:357–67 CrossRef Medline

3. Tofts PS, Brix G, Buckley DL, et al. **Estimating kinetic parameters from dynamic contrast-enhanced T(1)-weighted MRI of a diffusable tracer: standardized quantities and symbols.** *J Magn Reson Imaging* 1999;10:223–32 CrossRef Medline

4. Chawla S, Kim S, Dougherty L, et al. **Pretreatment diffusion-weighted and dynamic contrast-enhanced MRI for prediction of local treatment response in squamous cell carcinomas of the head and neck.** *AJR Am J Roentgenol* 2013;200:35–43 CrossRef Medline

5. Kim S, Loevner LA, Quon H, et al. **Prediction of response to chemoradiation therapy in squamous cell carcinomas of the head and neck using dynamic contrast-enhanced MR imaging.** *AJNR Am J Neuroradiol* 2010;31:262–68 CrossRef Medline

6. Jansen JF, Schöder H, Lee NY, et al. **Tumor metabolism and perfusion in head and neck squamous cell carcinoma: pretreatment multimodality imaging with 1H magnetic resonance spectroscopy, dynamic contrast-enhanced MRI, and [18F]FDG-PET.** *Int J Radiat Oncol Biol Phys* 2012;82:299–307 CrossRef Medline

7. Bernstein JM, Kershaw LE, Withey SB, et al. **Tumor plasma flow determined by dynamic contrast-enhanced MRI predicts response to induction chemotherapy in head and neck cancer.** *Oral Oncol* 2015;51:508–13 CrossRef Medline

8. Chawla S, Kim S, Loevner LA, et al. **Prediction of disease-free survival in patients with squamous cell carcinomas of the head and neck using dynamic contrast-enhanced MR imaging.** *AJNR Am J Neuroradiol* 2011;32:778–84 CrossRef Medline

9. Shukla-Dave A, Lee NY, Jansen JF, et al. **Dynamic contrast-enhanced magnetic resonance imaging as a predictor of outcome in head-and-neck squamous cell carcinoma patients with nodal metastases.** *Int J Radiat Oncol Biol Phys* 2012;82:1837–44 CrossRef Medline

10. Kim S, Quon H, Loevner LA, et al. **Transcytolemmal water exchange in pharmacokinetic analysis of dynamic contrast-enhanced MRI data in squamous cell carcinoma of the head and neck.** *J Magn Reson Imaging* 2007;26:1607–17 CrossRef Medline

11. Yankeelov TE, Lepage M, Chakravarthy A, et al. **Integration of quantitative DCE-MRI and ADC mapping to monitor treatment response in human breast cancer: initial results.** *Magn Reson Imaging* 2007;25:1–13 CrossRef Medline

12. Springer CS Jr, Li X, Tudorica LA, et al. **Intratumor mapping of intracellular water lifetime: metabolic images of breast cancer?** *NMR Biomed* 2014;27:760–73 CrossRef Medline

13. Li X, Cai Y, Moloney B, et al. **Relative sensitivities of DCE-MRI pharmacokinetic parameters to arterial input function (AIF) scaling.** *J Magn Reson* 2016;269:104–12 CrossRef Medline

14. Tudorica A, Oh KY, Chui SY, et al. **Early prediction and evaluation of breast cancer response to neoadjuvant chemotherapy using quantitative DCE-MRI.** *Transl Oncol* 2016;9:8–17 CrossRef Medline

15. Li X, Priest RA, Woodward WJ, et al. **Cell membrane water exchange effects in prostate DCE-MRI.** *J Magn Reson* 2012;218:77–85 CrossRef Medline

16. Lowry M, Zelhof B, Liney GP, et al. **Analysis of prostate DCE-MRI: comparison of fast exchange limit and fast exchange regimen pharmacokinetic models in the discrimination of malignant from normal tissue.** *Invest Radiol* 2009;44:577–84 CrossRef Medline

17. Chang EY, Li X, Jerosch-Herold M, et al. **The evaluation of esophageal adenocarcinoma using dynamic contrast-enhanced magnetic resonance imaging.** *J Gastrointest Surg* 2008;12:166–75 CrossRef Medline

18. Jajamovich GH, Huang W, Besa C, et al. **DCE-MRI of hepatocellular carcinoma: perfusion quantification with Tofts model versus shutter-speed model–initial experience.** *MAGMA* 2016;29:49–58 CrossRef Medline

19. Lee SH, Hayano K, Zhu AX, et al. **Water-exchange-modified kinetic parameters from dynamic contrast-enhanced MRI as prognostic biomarkers of survival in advanced hepatocellular carcinoma treated with antiangiogenic monotherapy.** *PLoS One* 2015;10:e0136725 CrossRef Medline

20. Ang KK, Harris J, Wheeler R, et al. **Human papillomavirus and survival of patients with oropharyngeal cancer.** *N Engl J Med* 2010;363:24–35 CrossRef Medline

21. Klussmann JP, Mooren JJ, Lehnen M, et al. **Genetic signatures of HPV-related and unrelated oropharyngeal carcinoma and their prognostic implications.** *Clin Cancer Res* 2009;15:1779–86 CrossRef Medline

22. Elrefaey S, Massaro MA, Chiocca S, et al. **HPV in oropharyngeal cancer: the basics to know in clinical practice.** *Acta Otorhinolaryngol Ital* 2014;34:299–309 Medline

23. Song HK, Dougherty L. **Dynamic MRI with projection reconstruction and KWIC processing for simultaneous high spatial and temporal resolution.** *Magn Reson Med* 2004;52:815–24 CrossRef Medline

24. Klaes R, Friedrich T, Spitkovsky D, et al. **Overexpression of p16(INK4A) as a specific marker for dysplastic and neoplastic epithelial cells of the cervix uteri.** *Int J Cancer* 2001;92:276–84 CrossRef Medline

25. Zhang Y, Poirier-Quinot M, Springer CS Jr., et al. **Active trans-plasma membrane water cycling in yeast is revealed by NMR.** *Biophys J* 2011;101:2833–42 CrossRef Medline

26. Nath KPR, Nelson DS, Pickup S, et al. **Acute changes in cellular-interstitial water exchange rate in DB-1 melanoma xenografts after lonidamine administration as a marker of tumor energetics and ion transport.** *Proc Intl Soc Magn Reson Med* 2014;22:2757

27. Koch CJ, Jenkins WT, Jenkins KW, et al. **Mechanisms of blood flow and hypoxia production in rat 9L-epigastric tumors.** *Tumor Microenviron Ther* 2013;1:1–13 CrossRef Medline

28. Cooper RA, Carrington BM, Loncaster JA, et al. **Tumour oxygenation levels correlate with dynamic contrast-enhanced magnetic resonance imaging parameters in carcinoma of the cervix.** *Radiother Oncol* 2000;57:53–59 CrossRef Medline

29. Layland MK, Sessions DG, Lenox J. **The influence of lymph node metastasis in the treatment of squamous cell carcinoma of the oral cavity, oropharynx, larynx, and hypopharynx: N0 versus N+.** *Laryngoscope* 2005;115:629–39 CrossRef Medline

30. Pineda FD, Medved M, Fan X, et al. **Comparison of dynamic contrast-enhanced MRI parameters of breast lesions at 1.5 and 3.0 T: a pilot study.** *Br J Radiol* 2015;88:20150021 CrossRef Medline